DECODING SATELLITE IMAGES OF EARTHQUAKES, PART-V: APPROXIMATING DERIVATIVES BY CONVOLUTIONS

Saumik Dana[1,*]

[1]*University of Southern California, Los Angeles, CA 90089*

*Address all correspondence to: Saumik Dana, E-mail: sdana@usc.edu

This document is part V of a series of documents providing a lowdown on image processing in the context of understanding satellite images of earthquakes.

KEY WORDS: *Earthquakes, satellite images, image processing, derivatives, convolutions*

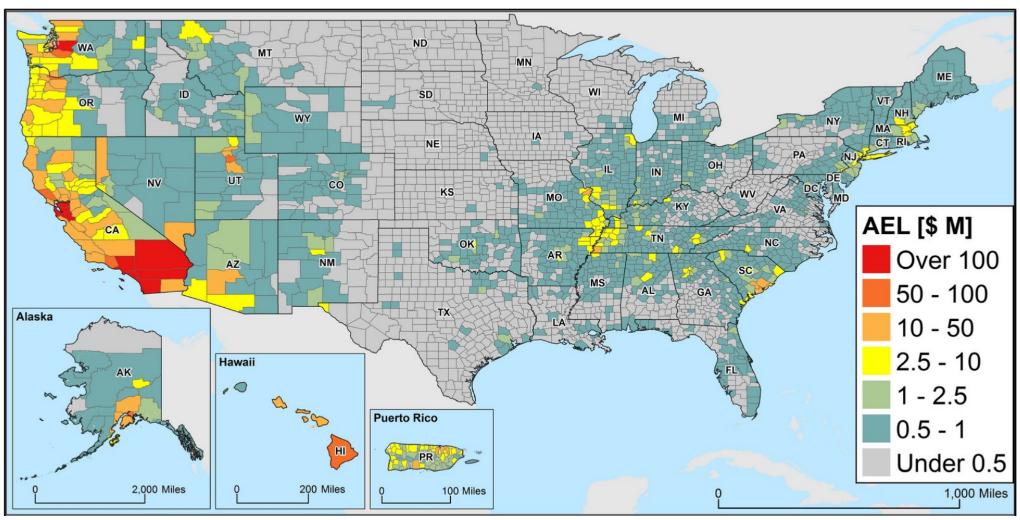

FIG. 1: Annualized Earthquake Losses (AEL: estimated long-term value of earthquake losses to the general building stock) by County. Sources: (1) https://www.usgs.gov/news/usgs-collaborates-fema-national-earthquake-loss-estimate and (2) https://www.fema.gov/hazus. The analysis yielded an estimate of the national AEL of $6.1 billion per year. Loss estimates based on the best science and engineering available (during 2016-2017). The study only addresses direct economic losses to buildings, and does not cover damage and losses to critical facilities, transportation and utility lifelines or indirect economic losses.

The earthquake cycle, from slow deformation associated with interseismic behavior to rapid deformation associated with earthquake rupture, spans spatial scales ranging from fractions of a meter associated with the size of contact asperities on faults and individual grains to hundreds of kilometers associated with plate boundaries (Kanamori and Brodsky (2004)). Similarly, temporal scales range from fractions of a second associated with slip at a point during earthquake rupture to hundreds of years of strain accumulation between earthquakes. In many cases, earthquakes are triggered after pore pressure perturbations activate critically stressed seismogenic faults (Kanamori and Brodsky (2004)), not just due to natural causes like earth tides (Scholz et al. (2019)), rainfall (Hainzl et al. (2006)), snowfall (Montgomery-Brown et al. (2019)), typhoons (Liu et al. (2009)), but also due to human activity (Foulger et al. (2018)). Ground motion and failure due to *earthquakes lead to huge losses to the tune of billions of dollars annually* *in the United States* (see Fig. 1). Understanding the causality between the events leading to fault slip, the location of the slipping fault and the earthquake recording is important for seismic design and monitoring of underground structures (Hashash et al. (2001)), bridges (Priestley et al. (1996)) and reinforced concrete buildings (Moehle (2015)) as well as climate mitigation projects like carbon sequestration (Zoback and Gorelick (2012)) and energy technologies like enhanced geothermal systems (Ellsworth et al. (2019)) or oilfield wastewater disposal (Keranen and Weingarten (2018)). A holistic framework would be to link the forward modeling framework going from quasi-static(Dana (2018, 2019a,b); Dana et al. (2018, 2020a); Dana and Lyathakula (2021); Dana et al. (2020b); Dana and Wheeler (2018a,b,c, 2019, 2020a,b)) to fully dynamic to the inverse modeling framework in the realm of remote sensing and image processing. The most critical aspect of image processing is the approximation of derivatives by convolution operations. In this document, we give a lowdown on how derivatives convert into convolutions, and how this singular simple operation is a game-changer in the realm of fusing computer vision with forward modeling. The game-changer is because ″convolution is the basis of convolutional neural networks″.

1. GOING FROM DERIVATIVES TO DIFFERENCING TO CONVOLUTION

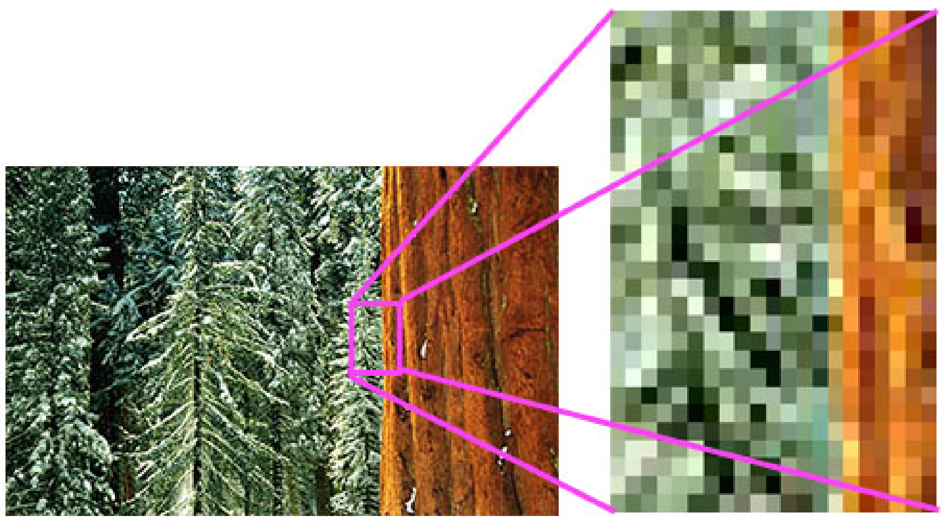

FIG. 2: The word ″pixel″ means a picture element. Every photograph, in digital form, is made up of pixels. They are the smallest unit of information that makes up a picture. Usually round or square, they are typically arranged in a 2-dimensional grid.

The partial derivative of a continuous function $f(x, y)$ with respect to the variable x is defined as the local slope of the plot of the function along the x direction or, formally, by the following limit:

$$\frac{\partial f}{\partial x} = \lim_{\Delta x \to 0} \frac{f(x + \Delta x, y) - f(x, y)}{\Delta x}$$

An image from a digitizer is a function of a discrete variable, so we cannot take Δx arbitrarily small: the smallest we can go is one pixel. If our unit of measure is the pixel, we have

$$\Delta x = 1$$

and a rather crude approximation to the derivative at an integer position j = x, i = y is therefore

$$\frac{\partial f}{\partial x}|_{j,i} \approx f(i, j + 1) - f(i, j)$$

Here we assume for simplicity that the origins and axis orientations of the x, y reference system and the i, j system coincide. Here is a piece of code that computes this approximation along row i in the image:

$$for(j = jstart; j <= jend; j++)h[i][j] = f[i][j+1] - f[i][j];$$

Notice, in passing, that the last value of j for which this computation is defined is the next-to-last pixel in the row, so jend must be defined appropriately. This operation amounts to taking a little two-cell mask g with the values

$$g[0] = 1 \qquad and \qquad g[1] = -1$$

in its two entries, placing the mask in turn at every position j along row i, multiplying what is under the mask by the mask entries, and adding the result. In C, we have

$$for(j = jstart; j <= jend; j++)h[i][j] = g[0]f[i][j+1] + g[1]f[i][j];$$

This adds a little generality, because we can change the values of g without changing the code. Since we are generalizing, we might as well allow for several entries in g. But clearly we will soon want to also combine pixels above i, j, not only on its sides, and for the whole picture, not just one row. This is easily done:

$for(i = istart; i <= iend; i++)for(j = jstart; j <= jend; j++)\{$
$h[i][j] = 0;$
$for(a = astart; a <= aend; a++)for(b = bstart; b <= bend; b++)h[i][j] += g[a][b]f[i-a][j-b];$
$\}$

where now g[a][b] is a two-dimensional array. The two innermost for loops just keep adding values to h[i][j],so we can express that piece of code by the following mathematical expression:

$$h(i,j) = \sum_{a=a_{start}}^{a=a_{end}} \sum_{b=b_{start}}^{b=b_{end}} g(a,b)f(i-a, j-b)$$

This is called a ″convolution″. Convolving a signal with a given mask g is also called filtering that signal with that mask. If ″f is a single point (the 1) in a sea of zeros i.e. a pixel in an image″ such that

$$f(i-a, j-b) = \delta(i-a, j-b) = \begin{cases} 1 & if\ i-a = j-b = 0 \\ 0 & otherwise \end{cases}$$

we get

$$h(i,j) = g(i,j)$$

so we get

$$h(i,j) = \sum_{a=a_{start}}^{a=a_{end}} \sum_{b=b_{start}}^{b=b_{end}} h(a,b)\delta(i-a, j-b)$$

Note that ″h can be any function″.

2. SMOOTHING

Computer vision operates on images that usually come in the form of arrays of pixel values. These values are invariably affected by noise, so it is useful to clean the images somewhat by an operation, called smoothing, that replaces

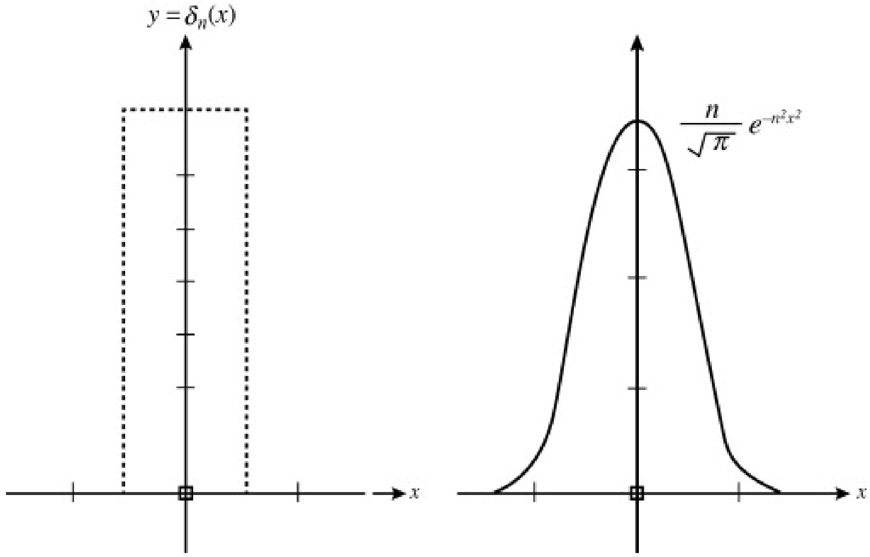

FIG. 3: Kronecker delta (left) versus Gaussian (right)

each pixel by a linear combination of some of its neighbors. This basically means that ″Kronecker delta $\delta(a, b)$ is replaced by Gaussian function $\gamma(a, b)$ which operates on a certain radius around (a, b) ″ such that

$$h(i, j) = \sum_{a=a_{start}}^{a=a_{end}} \sum_{b=b_{start}}^{b=b_{end}} h(a, b)\gamma(i - a, j - b)$$

Then all derivatives are expressed in terms of derivatives of the Gaussian

2.1 Why Gaussian?

- ✓ Gaussian is, by far the most popular smoothing function in computer vision
- ✓ The Gaussian is, as noted above, symmetric. It also emphasizes nearby pixels over more distant ones, a property shared by any nonincreasing function $\gamma(a, b)$. This property reduces smearing (blurring) while still maintaining noise averaging properties
- ✓ A more quantitative useful property of the Gaussian function is its smoothness. If $\gamma(a, b)$ is considered as a function of real variables a, b, it is differentiable infinitely many times. Although this property by itself is not too useful with discrete images, it implies that in the frequency domain the Gaussian drops as fast as possible among all functions of a given space-domain support. Thus, it is as low-pass a filter as one can get for a given spatial support. This holds approximately also for the discrete and truncated version of the Gaussian
- ✓ In addition, the Fourier transform of a Gaussian is again a Gaussian, a mathematically convenient fact
- ✓ Another important property of $\gamma(a, b)$ is that it never crosses zero, since it is always positive.

References

Dana, S., Addressing challenges in modeling of coupled flow and poromechanics in deep subsurface reservoirs, PhD thesis, The University of Texas at Austin, 2018.

Dana, S., A simple framework for arriving at bounds on effective moduli in heterogeneous anisotropic poroelastic solids, *arXiv preprint arXiv:1912.10835*, 2019a.

Dana, S., System of equations and staggered solution algorithm for immiscible two-phase flow coupled with linear poromechanics, *arXiv preprint arXiv:1912.04703*, 2019b.

Dana, S., Ganis, B., and Wheeler, M.F., A multiscale fixed stress split iterative scheme for coupled flow and poromechanics in deep subsurface reservoirs, *Journal of Computational Physics*, vol. **352**, pp. 1–22, 2018.

Dana, S., Ita, J., and Wheeler, M.F., The correspondence between voigt and reuss bounds and the decoupling constraint in a two-grid staggered algorithm for consolidation in heterogeneous porous media, *Multiscale Modeling & Simulation*, vol. **18**, no. 1, pp. 221–239, 2020a.

Dana, S. and Lyathakula, K.R., Uncertainty quantification in friction model for earthquakes using bayesian inference, *arXiv preprint arXiv:2104.11156*, 2021.

Dana, S., Srinivasan, S., Karra, S., Makedonska, N., Hyman, J.D., O'Malley, D., Viswanathan, H., and Srinivasan, G., Towards real-time forecasting of natural gas production by harnessing graph theory for stochastic discrete fracture networks, *Journal of Petroleum Science and Engineering*, vol. **195**, p. 107791, 2020b.

Dana, S. and Wheeler, M.F., Augmented lagrangian for treatment of hanging nodes in hexahedral meshes, *arXiv preprint arXiv:1809.04031*, 2018a.

Dana, S. and Wheeler, M.F., Convergence analysis of fixed stress split iterative scheme for anisotropic poroelasticity with tensor biot parameter, *Computational Geosciences*, vol. **22**, no. 5, pp. 1219–1230, 2018b.

Dana, S. and Wheeler, M.F., Convergence analysis of two-grid fixed stress split iterative scheme for coupled flow and deformation in heterogeneous poroelastic media, *Computer Methods in Applied Mechanics and Engineering*, vol. **341**, pp. 788–806, 2018c.

Dana, S. and Wheeler, M.F., Design of convergence criterion for fixed stress split iterative scheme for small strain anisotropic poroelastoplasticity coupled with single phase flow, *arXiv preprint arXiv:1912.06476*, 2019.

Dana, S. and Wheeler, M.F., An efficient algorithm for numerical homogenization of fluid filled porous solids: part-i, *arXiv preprint arXiv:2002.03770*, 2020a.

Dana, S. and Wheeler, M.F., A machine learning accelerated fe^2 homogenization algorithm for elastic solids, *arXiv preprint arXiv:2003.11372*, 2020b.

Ellsworth, W.L., Giardini, D., Townend, J., Ge, S., and Shimamoto, T., Triggering of the pohang, korea, earthquake (m w 5.5) by enhanced geothermal system stimulation, *Seismological Research Letters*, vol. **90**, no. 5, pp. 1844–1858, 2019.

Foulger, G.R., Wilson, M.P., Gluyas, J.G., Julian, B.R., and Davies, R.J., Global review of human-induced earthquakes, *Earth-Science Reviews*, vol. **178**, pp. 438–514, 2018.

Hainzl, S., Kraft, T., Wassermann, J., Igel, H., and Schmedes, E., Evidence for rainfall-triggered earthquake activity, *Geophysical Research Letters*, vol. **33**, no. 19, 2006.

Hashash, Y.M., Hook, J.J., Schmidt, B., John, I., and Yao, C., Seismic design and analysis of underground structures, *Tunnelling and underground space technology*, vol. **16**, no. 4, pp. 247–293, 2001.

Kanamori, H. and Brodsky, E.E., The physics of earthquakes, *Reports on Progress in Physics*, vol. **67**, no. 8, p. 1429, 2004.

Keranen, K.M. and Weingarten, M., Induced seismicity, *Annual Review of Earth and Planetary Sciences*, vol. **46**, pp. 149–174, 2018.

Liu, C., Linde, A.T., and Sacks, I.S., Slow earthquakes triggered by typhoons, *Nature*, vol. **459**, no. 7248, pp. 833–836, 2009.

Moehle, J., *Seismic design of reinforced concrete buildings*, McGraw-Hill Education, 2015.

Montgomery-Brown, E., Shelly, D.R., and Hsieh, P.A., Snowmelt-triggered earthquake swarms at the margin of long valley caldera, california, *Geophysical Research Letters*, vol. **46**, no. 7, pp. 3698–3705, 2019.

Priestley, M.N., Seible, F., and Calvi, G.M., *Seismic design and retrofit of bridges*, John Wiley & Sons, 1996.

Scholz, C.H., Tan, Y.J., and Albino, F., The mechanism of tidal triggering of earthquakes at mid-ocean ridges, *Nature communications*, vol. **10**, no. 1, pp. 1–7, 2019.

Zoback, M.D. and Gorelick, S.M., Earthquake triggering and large-scale geologic storage of carbon dioxide, *Proceedings of the National Academy of Sciences*, vol. **109**, no. 26, pp. 10164–10168, 2012.